Radiowave Phase Scintillation and Precision Doppler Tracking of Spacecraft

J. W. Armstrong

Jet Propulsion Laboratory, California Institute of Technology
Mail Stop 238-725; 4800 Oak Grove Dr.
Pasadena CA 91 109; United States

Short Title: Phase Scintillation and Precision Doppler

Submitted to: *Radio Science*

November 24, 1997

ABSTRACT

Phase scintillation caused by propagation through irregularities in the solar wind, ionosphere, and troposphere, introduces noise in spacecraft radio science experiments. In precision Doppler tracking observations, scintillation can be the dominant noise source; statistics of this propagation noise are necessary for experiment planning and in design of optimum signal processing procedures. Here high-precision tracking data taken with operational spacecraft (Mars Observer, Galileo, Mars Global Surveyor) and ground systems are used to produce temporal statistics of tropospheric and charged particle phase scintillation. Using the differing transfer functions to the Doppler observable, the variance of Doppler frequency fluctuations is approximately decomposed into two propagation processes. The first, associated with distributed scattering along the sight-line in the solar wind, has a smooth spectrum. The second, associated principally with localized tropospheric scattering for X-band experiments, has a marked autocorrelation at the two-way light time between the earth and the spacecraft (thus a cosine-squared modulation of the fluctuation power spectrum). For the X-band data, taken in the antisolar hemisphere, the average noise levels of this process are in good agreement with average tropospheric noise levels determined independently from water vapor radiometer observations and radio interferometic data. The variance of the process having a smooth spectrum is consistent with charged-particle noise levels determined independently by dual-frequency observations of the Viking spacecraft made at comparable sun-earth-spacecraft angles. The observations reported here are used to refine the propagation noise model for Doppler tracking of deep space probes. In particular they can be used to predict propagation noise levels for high precision X- and Ka-band tracking observations (e.g. atmosphere/ionosphere/ring occultations, celestial mechanics experiments, gravitational wave experiments) to be done using the Cassini spacecraft.

1. Introduction

Precision radio science experiments with spacecraft have been used in a variety of geophysical, planetary and astronomical investigations. These include studies of planetary mass distributions, electron densities of planetary ionospheres, pressure-temperature profiles of planetary atmospheres, planetary shapes, distribution of planetary ring material, and tests of relativistic gravity [e.g., Estabrook and Wahlquist, 1975; Reasenberg *et al.*, 1979; Vessot *et al.*, 1980; Marouf et *al.*, 1986; Theme, 1987; Tyler *et al.*, 1992; Anderson et *al.*, 1996; Kursinski, 1996]. Instrumental noises can often be made extraordinarily small and the ultimate sensitivity of these experiments is then determined by other factors.

An important noise source in precision Doppler tracking is phase scintillation caused by wave propagation through the irregular media--solar wind, ionosphere, and troposphere--between the spacecraft and the tracking station [e.g., Armstrong, Woo, and Estabrook, 1979, 1980; Sramek, 1989; Keihm, 1995]. At high enough radio frequencies, the effect of the (dispersive) charged particle scintillation can be made small, leaving (non-dispersive) tropospheric scintillation as an increasingly important noise source. Tropospheric scintillation statistics are required for experiment planning, error budgets, and for algorithm design to discriminate signals from noise.

This paper has two goals. First, statistics of tropospheric and charged particle scintillation on earth-spacecraft paths in the antisolar direction are inferred from precision tracking data on operational spacecraft (Mars Observer, Galileo, Mars Global Surveyor). Second, these statistics are used to verify the propagation noise model for precision X- and Ka-band Doppler tracking observations. The paper is organized as follows. In section 2, the transfer functions of scintillation and other noises to the Doppler observable are reviewed. In section 3, the observations are discussed. In section 4, temporal autocorrelation functions of the

Doppler frequency residuals are presented and the differing transfer functions for tropospheric and solar wind scintillation used to estimate the variance of each process. Sections 5 and 6 discuss applications, including prediction of propagation noise for tracking experiments and relevance to optimal filtering in the presence of propagation and antenna mechanical noises. Particular attention is given to implications for the high-sensitivity X- and Ka-band experiments on the Cassini mission. Section 7 contains the summary and conclusions.

2. Transfer Functions

In "two-way" spacecraft tracking, the ground station simultaneously transmits to and receives from the spacecraft nominally monochromatic signals. The transmitted signal ("uplink") is received at the spacecraft and is transponder (multiplied in frequency by the transponder ratio, α, preserving the phase of the uplink), producing a signal ("downlink") that is radiated back to the earth. This downlink is received at the earth; its frequency is compared with the frequency of a signal derived from the current uplink, multiplied in frequency by the transponder ratio. The result is that the phase of the received signal is compared with the phase of the transmitted signal at a time 2L/c earlier (L = earth-spacecraft distance). The time derivative of this phase time series, after correcting for known spacecraft-earth motion and other effects, is the residual two-way Doppler frequency. In the absence of noise and systematic errors this residual would be zero.

Analysis of the noises affecting high-sensitivity Doppler experiments have been published, for example, by Wahlquist et *al. [1977],* Estabrook [1978], Peng et *al. [1988),* Armstrong [1989], and Riley [1990]. The noise sources usually considered are propagation noise (tropospheric and charged particle scintillation), ground electronics noise (frequency standard and frequency distributions, transmitter, receiver), antenna mechanical noise, thermal noise, and spacecraft noise (electronics and unmodeled motion of the spacecraft). These noises

enter the observable in different ways [Estabrook, 1978; Vessot and Levine, 1978]. In this section the transfer functions of tropospheric and charged particle scintillation are reviewed, as are those of frequency standard noise and antenna mechanical noise (which can potentially be confused with tropospheric scintillation).

In Figure 1, adapted from Estabrook [1978], transfer functions are illustrated by space-timc diagrams for the cases of frequency standard noise, antenna mechanical noise, tropospheric scintillation, and charged particle (ionospheric and solar wind) scintillation. This diagram takes into account the non-unity transponder ratio. (Spacecraft transponder ratios are 240/221 for S-band up/S-band down, 880/22 1 for S-band up/X-band down, 880/749 for X-band up/X-band down, 3344/749 for X-band up/Ka-band down, and 14/15 for Ka-band up/Ka-band down on the Cassini spacecraft.) Figure 1 is a collection of space-time diagrams (space vertically, showing the separation L between the earth and the spacecraft) and time horizontally. Radio waves transmitted to and received from the spacecraft are shown as dashed lines. Beneath each space-time diagram is a schematic plot of the times series of frequency fluctuation in the two-way Doppler produced for each effect.

Frequency standard ("clock") noise is irregularity in the master oscillator controlling the transmitter/receiver systems. Because the Doppler observable is the difference between the transmitted and received frequencies, a clock frequency perturbation is seen immediately as a perturbation in the uplink frequency of the signal mixed with the downlink. It thus appears in the observed Doppler, scaled by the transponder ratio. After a time T_2 = 2L/c = the two-way light time to the spacecraft, the original frequency perturbation will have been transponder (i.e., scaled by α) and sent back to the Earth, resulting again in a difference between transmitted and received frequencies. This second event has the same absolute value as the original perturbation, but since it enters now in the receiver signal chain it has the opposite sign in the two-way Doppler. Thus clock noise enters the Doppler observable as the convolution of the actual time

series of frequency standard fluctuations with a transfer function proportional to $[\delta(t) - \delta(t-T_2)]$. The signature of a time series dominated by clock or clock-like noise is a negative-going autocorrelation function (acf) at time lag $\tau = T_2$, with the absolute amplitude of the acf at $\tau = T_2$ depending on the spectral shape of the clock noise process.

Tropospheric scintillation has a transfer function identical to that of antenna mechanical noise. A refractive index fluctuation over the station perturbs the phase of both the uplink and downlink waves propagating through it, as shown. Since tropospheric refractivity variations, dominated by water vapor fluctuations, are nondispersive at microwave frequencies, the phase shift through the blob is proportional to radio frequency. Suppose that the transmitted frequency is f. so that the (unperturbed) downlink frequency is (a f_o). Then the troposphere-induced phase perturbation on the downlink is proportional to *(a* f_o) while the phase perturbation on the uplink is proportional to f_o. The two-way Doppler is immediately affected as phase-perturbed downlink is compared with the reference frequency (a f_o). As the uplink is transponder at the spacecraft, the tropospheric phase fluctuation is preserved and coherently multiplied by the transponder ratio. Thus the downlink has a phase perturbation proportional to (a f_o). This is compared with the reference frequency *(a* f_o) producing a second "pulse" in the Doppler record with the same magnitude and sign as the initial perturbation, but a two-way light time later. The observed Doppler time series is the convolution of the fluctuations that would have been observed on one passage through the random medium with the transfer function $[\delta(t) + \delta(t-T_2)]$, indistinguishable (based on the form of the transfer function only) from antenna mechanical noise.

Antenna mechanical noise in the ground station (say due to unmodeled motion of the antenna as it tracks the spacecraft) produces a different two-pulse response. If the ground station were effectively pushed toward the spacecraft, the received wave is blue-shifted with respect to the frequency standard with a resulting immediate effect in the Doppler. The transmitted wave is

however also blue shifted due to the motion of the station toward the spacecraft. A two-way light time later the transponded wave arrives, blue shifted with respect to the frequency standard. Thus ground station buffeting noise enters the Doppler observable as the convolution of the buffeting time series with a transfer function proportional to $[\sim(t) + \delta(t-T_2)]$. The signature of a time series dominated by ground station buffeting noise would be a positive-going autocorrelation at lag T_2, with amplitude that depends on the spectrum of the antenna mechanical noise process.

Charged particle scintillation arising from a refractive index fluctuation at a distance x from the earth is also illustrated in Figure 1. A refractive index fluctuation perturbs the phase of both the uplink and downlink waves propagating through the fluctuation, as shown. Because the refractivity of a cold, unmagnetized plasma is proportional to (radio frequency)$^{-2}$, the phase shift through the plasma blob is proportional to (radio frequency)$^{-1}$. As before, let the transmitted frequency be f. and so that the (unperturbed) downlink frequency is a f_o. The plasma blob perturbs the downlink phase proportional to $(\alpha f_0)^{-1}$ while the phase perturbation on the uplink is proportional to $(f_0)^{-1}$. The two-way Doppler is affected when the phase-perturbed downlink is compared with the reference frequent y a f., producing an event in the two-way Doppler proportional to $(\text{CX}\, f_0)^{-1}$. As the uplink is transponder at the spacecraft, the plasma phase fluctuation seen on the uplink is preserved and coherently multiplied by the transponder ratio. Thus the downlink has a phase perturbation proportional to a $(f_0)^{-1}$. When the downlink is compared with the reference frequency α f. there is a second event in the Doppler, with magnitude proportional to α (fO)-l. The second event follows the first by a time 2 (L-x)/c. The effect of a plasma fluctuation at a distance x from the earth in the Doppler is a two-pulse response: the observed Doppler time series is the convolution of the plasma fluctuations that would have been observed on one passage through the plasma fluctuation with a transfer function proportional to $[\alpha^{-1}\ \delta(t) + a\ \delta(t-2(L-x)/c)]$, where L is the earth-spacecraft distance. For ionospheric scintillation, $x \lesssim 100$ km = 0.3 msec of light travel time, much less than the 10

second integration time of the measurements presented here and the effective transfer function for ionospheric Scintillation is the convolution with a function proportional to $[\alpha^{-1}\delta(t) + \alpha\,\delta(t-T_2)]$. For the extended solar wind, the effect is the integral over screen position, x, with screens weighted by the magnitude of the solar wind irregularities along the line-of-sight through the interplanetary medium. Model calculations for a Kolmogorov density fluctuations in the solar wind, with variance proportional to (distance from the sun)$^{-4}$, and sun-earth-spacecraft angles $\approx$ 100o show that the superposition of the scattering in this extended medium effectively suppresses any signature in the temporal autocorrelation function.

3. Observations

The radio science investigations of Mars Observer, Galileo, and Mars Global Surveyor, and description of the radio science system are given by Tyler et *al. [1992]* and Anderson *et al.* [1992]. The observations were principally made 1993 March 22-April 9 (MO), 1993 March 22-April 11 (GLL), and 1997 April 14-May 4 (MGS); isolated tests were done outside these intervals. All data were taken with the spacecraft in transfer orbits to their target planets. The 1993 MO/GLL observations were part of a coincidence experiment to search for low-frequency gravitational waves. The Deep Space Network (DSN) tracked all spacecraft, using the 34-m High-Efficiency (HEF) antennas (MO and MGS) and the 70-m antennas (GLL). MO and MGS observations were made at X-band on both the up- and downlinks; GLL observations were at S-band. The tracking stations have been engineered for excellent instrumental frequency stability and the electronics were referenced to hydrogen-maser frequency standards; the result was very

---

1 Of the four processes that produce features in the autocorrelation of the Doppler time series exactly at the two-way light time, only ionospheric scintillation does not have a time-symmetric transfer function. For some values of the transponder ratio the transfer function can be significantly non-symmetric. This suggests that, in principle, ionospheric scintillation could be distinguished from the other processes based on analysis of the third order lagged product, $\langle x(t)\, x(1+\tau_1)\, x(t+\tau_2)\rangle$, or its Fourier transform, the bispectrum [e. g., Armstrong 1977; MacDonald 1989]. In practice, the data collected here have third central moments very close to zero, and such a procedure is not impractical.

low phase noise from the instrumentation [Peng *et al.* 1988]. For MO and MGS, the received pre-detection electric field was down-converted to baseband, sampled using the Radio Science Subsystem [Asmar and Renzetti, 1993], and the signal phase and frequency fluctuations extracted in software. For GLL, the phase was extracted in hardware using the standard tracking receivers. Using engineering telemetry, the MO data were corrected to account for spacecraft antenna motion caused by systematic effect in the reaction wheels used to orient the spacecraft. GLL was observed using its low-gain antenna and no corrections for spacecraft systematic were required in the 0-0.05 Hz Nyquist band considered here. Owing to improved design and better placement of the antenna relative to spacecraft center-of-mass, no corrections for the reaction wheels were required for the cruise MGS data.

Except for isolated tests, all data were taken when the spacecraft were in the antisolar hemisphere. During the principal observations, the sun-earth-spacecraft (elongation) angle varied from 101o to 920 (MO), 1550 to 1380 (GLL), and 1240 to 1130 (MGS). The two-way light times changed between 937 to 1128 seconds for MO, 669 to 915 seconds for GLL, and 479 to 631 seconds for MGS. The MO and MGS observations are the only X-band up- and downlink observations to date made in the antisolar hemisphere--thus solar plasma scintillation effects were reduced relative to earlier tracking data taken either with raypaths toward the sun or with lower radio frequencies.

4. Scintillation Statistics

4.1 *Autocorrelation functions of the frequency residuals*

Figure 2 shows a temporal autocorrelation function and power spectrum for MGS frequency residuals taken on 1997 DOY 108. The two-way light time was 504 seconds and the

elongation angle was 1220. The data have been high-pass filtered at 0.001 Hz. Note the well-defined peak in the correlation function at the two-way light time. The inset plot is the power spectrum of the data, plotted on linear scales and with $1/T_2$ as the unit of frequency. The clear spectral modulation--nulls at odd multiples of $1/(2\ T_2)$--is a consequence of the positive correlation at time lag T_2. Positive correlation at $\tau = T_2$ is observed in $\gtrsim$ 90% in the X-band (MO and MGS) data, with the magnitude of the correlation at T_2 varying from greater than 0.4 to less than 0.1 over the course of the approximately three weeks of observation. (The remaining $\lesssim$ 10% of the data either have marginal features at $\tau = T_2$ or very poorly determined acfs.)

Figures 3, 4, and 5 show autocorrelation functions of GLL data taken on 1993 DOYS 091,090, and 098. (The GLL data have been high-pass filtered at 0.001 Hz. Also, because of the lower SNR on the GLL downlink, the GLL data have been low-pass filtered to 0.01 Hz prior to spectral/correlation analysis to improve the SNR of propagation processes relative to thermal noise. This is principally responsible for the wider GLL acfs in Figures 3, 4, and 5 compared with Figure 2.) About 60% of the time, the S-band data show discernible positive correlation at T_2 (compare, e.g., Figures 3 and 4). Very rarely, a positive correlation at a lag smaller than T_2 (see Figure 5) is observed. This is presumably the result of an enhanced, spatially well-defined, scattering region in the solar wind.

As discussed in Section 2, four noise processes give non-zero autocorrelation values at the two-way light time: clock noise, antenna unmodeled motion, tropospheric scintillation, and ionospheric scintillation. A localized region of significantly enhanced plasma variation in the solar wind along the earth-spacecraft sight-line can cause an autocorrelation peak at $\tau < T_2$. The true frequency of occurrence of such features, which might be corotating with the sun, cannot be determined from these observations (the total approximately three week observation time is less than one solar rotation), but at least one was observed. (Also, observations in the antisolar direction may not be best for detecting such features in radio data). Model calculations show that

the integrated effect for a spacecraft at sun-earth-probe angle ≈100° viewed through a spherically symmetric solar wind having electron density variance proportional to (distance from the sun)$^{-4}$ is to produce an essentially featureless autocorrelation function.

Clock noise gives negative correlations at a lag of T_2. Independent measurements of the hydrogen masers and frequency distribution system show that this process has a variance typically 1.5 orders of magnitude smaller than the variance of the data. Clock noise is thus negligible here.

Unmodeled motion of a DSN 34-m beam-waveguide ground antenna (a different design than the 34-m HEF antennas used here) was measured in tests where the antenna was stationary [Otoshi et *al.*, 1994]. Those tests showed unmodeled motion at levels too small to be important in the MO or MGS data. There have been no engineering measurements made on the 70-m antenna to isolate the antenna mechanical noise contribution at the levels of interest here.

S-band ionospheric scintillation apparently plays a variable but non-negligible role, at least for the GLL S-band observations taken at elongations ≈145°. The T_2-correlation in the S-band data, while not always clearly observed, is probably caused by the ionosphere. (If the T_2-correlated process seen in the S-band data were troposphere, then the variance of the frequency fluctuations at X-band would be much larger than are observed by MO and MGS. If unmodeled motion of the 70m antenna were dominating the ionosphere, then a T_2-correlation would presumably be observed as a consistently reproducible instrumental effect, which it is not.)

4.2 *Tropospheric and Solar Wind Scintillation Levels for X-Band Tracking*

Measurements of ground and spacecraft instrumental noises prior to the MO X-band experiment suggested that propagation noise would dominate the observed frequency

fluctuations. Since tropospheric scintillation enters the two-way Doppler via convolution with $[\delta(t) - \delta(t-T_2)]$, the spectrum of frequency fluctuations is modulated by $\cos^2(\pi f T_2)$. That is, the spectrum of a Doppler time series dominated by tropospheric scintillation will have sharp nulls at Fourier frequencies which are odd multiples of $1/(2 T_2)$. At these frequencies the noise from extended plasma scintillation should dominate. This suggests a simplification of the model that would be consistent with most of the variance on a typical track: the variability in the time series is mainly due to tropospheric scintillation and extended plasma scintillation only.

Within the idealization that the fluctuations are all due to propagation noise, the variance of the X-band time series can be decomposed, based on the spectrum, into two components--a smooth continuum ("solar wind") and a $\cos^2(\pi f T_2)$ modulated component ("troposphere"). Using Simpson's rule for integration, and integrating over the $N \approx 50$ peaks of the modulation out to the 0.05 Hz Nyquist frequency, the variance in the continuum can be estimated from the spectrum of frequency fluctuations, S(f): $\mathrm{var(continuum)} = \sum_{k=1}^{N} S(f = k/T_2 + 1/2T_2)\, 1/T_2$. Similarly, at the Fourier frequencies where $\cos^2(\pi f T_2)$ has peaks, the spectral levels are the sum of the local propagation and continuum noises. Thus (the factor of 2 is due to the average value of cosine-squared), the tropospheric noise can be estimated via: $2\ \mathrm{var(local\ propagation)} = \sum_{k=1}^{N} S(f = k/T_2)\, 1/T_2 - \mathrm{var(continuum)}$. This decomposition would be expected to overestimate both the solar wind and tropospheric variances. This is because the estimated "troposphere" includes ground antenna buffeting and ionosphere at some level and the estimated "solar wind" includes all continuum processes.

Figure 6 shows the result of this decomposition under these simplifying assumptions. The estimated square-root Allan variance [Barnes et *al.* 1970] at 100 second integration times is plotted as a function of time during the 1993 MO observations, assuming white tropospheric frequency fluctuations in the band 0,0005-0.05 Hz to convert variance to Allan variance. Where

the inferred tropospheric level was comparable to the expected error, it is plotted as an upper limit. Note the slightly different vertical scales for the X-band solar wind and tropospheric processes and the rather large variability of the inferred tropospheric process. Overplotted in the lower panel, as a dotted region, is the average tropospheric level determined from analysis of independent water vapor radiometer (WVR) data at Goldstone [Keihm, 1995]. Overplotted on the upper panel is a dotted line showing the average X-band charged particle effect at elongation =100o, as estimated from dual-frequency Viking data [Armstrong, Woo, and Estabrook 1979, 1980]. The general agreement between the inferred tropospheric component and the WVR data is good, as is the inferred solar wind component and the Viking data taken at similar elongations. Evidently the tropospheric variance, in particular, is nonstationary and has a large skewness to its distribution.

5. Applications to Precision X- and Ka-Band Doppler Observations

These observations can be used to confirm and refine the noise model and to predict propagation noise levels in precision deep space tracking experiments. It is conventional [Barnes *et al.* 1970] to consider the statistics of the non-dimensional time series of fractional frequency fluctuations, $y(t) = \Delta f(t)/f_0$. For very high-precision two-way radio science observations, e. g. the search for low-frequency gravitational waves, the variability of $\Delta f(t)/f_0$, after deterministic effects (such as orbital signature) have been removed, can be modeled as the sum of propagation noise, antenna mechanical noise, clock noise, unmodeled motion of the spacecraft antenna, ground electronics noise, thermal noise, spacecraft electronics noise, spacecraft buffeting noise, systematic errors, and desired signal (each with its appropriate transfer function) [Armstrong 1989]. Here “thermal” is noise due to finite SNR in the radio links, and “signal” is the desired radio science signal in the two-way time series (e.g., for gravitational waves the signal is related to the earth-source-spacecraft geometry and the polarization state of the wave [Estabrook and

Wahlquist 1975, Wahlquist 1987]). A noise model for precision Doppler tracking was developed by Riley et *al. [1990]*. The observations reported here can refine the propagation component of this noise model using data taken under operational conditions.

The Mars Observer data (Figure 6 upper panel) imply that Ka-band noise from plasma irregularities having a Kolmogorov spectrum and observed at solar elongation angles $\varepsilon > 160^{o}$ will have a square-root Allan variance $\sigma_y(1000\ \text{sec}) \approx 9 \times 10^{-16}$ and $\sigma_y(10{,}000\ \text{sec}) \approx 6 \times 10^{-16}$. The tropospheric noise (Figure 6, lower panel) was observed with Mars Observer in spring/fall 1993 and typically between about sunset and early morning, local time, at each tracking complex. Although there is evidence for seasonal and diurnal dependence [Sramek 1989], the Mars Observer data in Figure 6 imply a skewed distribution function of tropospheric noise with an average value[1] of $\sigma_y(1000\ \text{sec}) \approx 3 \times 10^{-14}$. This average level is in good general agreement with WVR [Keihm 1995] and with interferometric data [Rogers *et al.* 1984; Sramek 1989] (under plausible assumptions about frozen flow and wind speed). It also underscores the necessity of good tropospheric calibration in order to achieve the Cassini end-to-end sensitivity requirement of $\sigma_y(1000\ \text{sec}) \approx 3 \times 10^{-15}$.

Gravitational wave experiments are concerned with the plasma propagation noise level near solar elongation angles ≈1 800. Plasma noise at other elongation angles is relevant for atmosphere, ionosphere, or ring occultation [e.g. Marouf et *al.* 1986; French *et al.* 1988; Kliore et *al.* 1997] and celestial mechanics [e.g. Comoretto *et al.* 1992; Bertotti *et al.* 1993; Schubert *et al.* 1994, Rappaport *et al.* 1997] observations. The noise levels for these experiments can be estimated based on a model of the solar wind/ionosphere elongation dependence [Armstrong Woo, and Estabrook 1979, 1980]. The X-band observations presented here are consistent with

[1] The tropospheric noise values are determined from the spectral decomposition described in Section 4. In particular, any antenna mechanical noise in the 34-m HEF antennas enters in the estimated tropospheric noise level. The agreement with other (purely tropospheric) data sets suggests that the antenna mechanical contribution is small compared with the troposphere. However antenna mechanical noise levels approaching 1 X 10⁻14 in 1000 second integrations could be present without significantly affecting the agreement with other data sets.

S/X data and model given by Armstrong Woo, and Estabrook [1979, 1980], Figure 2 (which shows AlIan deviation and phase spectral density at 0.001 Hz as a function of elongation for charged particles). For spacecraft observations (with the exception of the *Solar Probe* mission), the velocity of the solar wind dominates the velocity of the spacecraft and one can simply scale (in radio frequency, by f_0^{-2}) observations taken at the same solar elongation angle (e.g., Figure 2 of Armstrong Woo, and Estabrook [1979, 1980], appropriate for "one-way" passage through the solar wind). To predict temporal plasma noise for observations of a spacecraft behind the sun form the data presented here, one needs to make assumptions about radial variation and the conversion of spatial structures to temporal variations. The data given here can be scaled to other elongations via numerical integrations through the extended solar wind, assuming density variance proportional to (solar distance)$^{-4}$ and assuming that the solar wind speed is radial everywhere along the line of sight; this procedure agrees well with data taken over a wider elongation range [Armstrong, Woo, and Estabrook 1979].

6. Other Applications

6.1 *Signal Processing in the Presence of Propagation Noise*

Spectra of noises are required to design filters which discriminate signals from noises and to predict achievable signal-to-noise ratios (SNRs). The SNR of a filter matched to a signal s(t) in the presence of noise having spectral density $P_N(f)$ is [e.g., Helstrom 1968]:

$$SNR = \int_{-\infty}^{\infty} \frac{|\tilde{s}(f)^2|}{P_N(f)}\, df$$

where $\tilde{s}$ is the Fourier transform of the signal. The spectral transfer function for propagation noise (and antenna mechanical noise) has sharp minima which, since the spectrum of the noise appears in the denominator of the above equation, suggests that SNR might be significantly improved if the Fourier transform of the signal has power at the frequencies of these minimal.

The X-band data (e.g., Figure 2) show clear spectral modulation due to the troposphere. At Ka-band, the plasma continuum will be further reduced and the contrast between spectral maxima and minima, prior to WVR calibration, will be more pronounced. Even after calibration, residual troposphere and antenna mechanical noise are likely to be an important noise sources. Exploitation of the minima at odd multiples of $1/(2\ T_2)$ in selected S-band data has been done as a proof-of-concept to estimate the continuum levels of secondary noise sources [Armstrong 1989]; this has applications in constraining the level of any stochastic background of gravitational waves in the millihertz band. Explicit use of this spectral modulation (and that of competing noise sources) in the search for candidate signals is required for best SNR; this is discussed by Tinto and Armstrong[1997].

6.2 *Tim and Frequency Transfer Between Ground and Space*

Comparison between precision frequency standards on the ground and on space probes is complicated by propagation through the troposphere, ionosphere, and solar wind. In addition to frequency comparison and transfer, precision time transfer can be important in e.g. orbiting VLB1 observations [D'Addario 1991]. The most precise comparison to date was achieved in the Gravity Probe A gravitational redshift experiment, which compared hydrogen masers on the

---

[1] The equation for matched filter SNR suggests that the SNR could be infinite if the signal power is non-zero at a null of the propagation or antenna mechanical noise spectrum. However the a finite length of a real data set can be views at as multiplication of an infinite data set by a temporal window, which implies that the spectrum is convolved with an associated spectral window [Jenkins and Watts 1969]. This "fills in" the nulls, making thcm non-zero. For suitable temporal windowing of the data, the ratio of the power at the frequencies of the propagation "nulls" to the power at the frequencies where the propagation noise is largest can be made to go as $(T_2/T)^2$, where T is the duration of the data set. Of course one may reach the level of secondary continuum noise sources before this depth-of-null in the propagation/antenna mechanical noise is achieved.

ground and on a suborbital spacecraft [Vessot *et al.* 1980]. Variants on this experiment have been proposed involving a spacecraft in elliptical earth orbit (observations on multiple orbits would be used to improve the redshift measurement) or on spacecraft sent deep into the sun's gravitational potential. At σ_y(100-1000 see) ≈ several X 10^{-14}, raw tropospheric noise is much larger than the intrinsic stability of modern frequency standards. In the Gravity Probe A experiment, tropospheric scintillation noise was largely removed by forming the difference between the one-way Doppler and one-half of the two-way Doppler as an observable [Vessot and Levine 1978]. This procedure exactly cancels the troposphere when T_2 = O. For non-zero T_2, as in observations of highly elliptical orbiters or of spacecraft sent close to the sun, there is a residual error in this observable that becomes increasingly important as the intrinsic stability of clocks improves. Explicit use of the transfer function can be used in the design of noise-canceling strategies (e.g. Vessot 1997). The required level of tropospheric cancellation can be determined from WVR data (Keihm 1995), interferometric observations (e. g., Rogers *et al.* 1984, Sramek 1990), or the tropospheric data given here from spacecraft observations, all of which are in general agreement.

6.3 *Radio Interferometric Effects*

The discussion in this paper has been in terms of the temporal statistics of the phase/frequency fluctuations. More directly relevant to precision geodesy with microwave interferometry or image formation through a turbulent atmosphere are the spatial statistics. Under assumptions (frozen flow, assumed pattern velocity) the spatial and temporal statistic for tropospheric radiowave scintillation can be related [e.g., Armstrong and Sramek 1982], Rogers *et al.* 1984, Sramek 1989, Wright 1996]. The data presented here are in good general agreement with interferometric determinations [e.g., Rogers *et al.* 1984, Sramek 1989].

7. Summary and Conclusions

High-quality Doppler observations of the Galileo, Mars Global Surveyor, and Mars Observer spacecraft have been analyzed to assess tropospheric and charged particle scintillation for observations made in the antisolar hemisphere using operational spacecraft and ground systems. Autocorrelation functions of the X-band observations show marked positive correlation at the two-way light time to the spacecraft. This autocorrelated process is interpreted as tropospheric scintillation. Under simplifying assumptions, and using the differing transfer functions for tropospheric and solar wind scintillation, the variances of these two processes are determined. The level and variability of the inferred plasma process is in good agreement with that expected for solar wind plasma at X-band and elongations ≈100 degrees. The average tropospheric variance is comparable to the average variance of the continuum X-band solar wind plasma noise at elongation ≈100 degrees. The average Allan variance associated with the tropospheric process is consistent with the average level of recent water-vapor turbulence measured at Goldstone and also consistent with values determined from radio interferometric data. The scatter in the tropospheric noise level is large, however, with the distribution skewed to a larger number of low-variance intervals and a fewer number of high-variance intervals. This variability in the turbulence level of the tropospheric process is too large to be due to estimation error only and presumable reflects real, nonstationary variation on time scales -hours.

These data show that uncorrected Cassini tracking data (Ka-band up- and downlink) will be dominated by tropospheric noise. The distribution of tropospheric noises and the agreement between the levels of tropospheric scintillation determined here and those determined independently with water vapor radiometers indicates that much of this variation will be correctable through WVR calibrations. The transfer-function modulation of antenna mechanical and residual tropospheric noise spectra can be used in filter design to improve detection probability of signals embedded in this noise.

Acknowledgment

The precision Doppler tracking capability described here is the result of work by many people. Crucial roles were played by colleagues in the NASA Deep Space Network, in the Galileo, Mars Observer, and Mars Global Surveyor Flight Projects, and in the Radio Science and Radio Science Support Teams; the contributions of these individuals are gratefully acknowledged. The data used here are from joint Mars Observer/Galileo/Ulysses observations made in 1993 by B. Bertotti, F. Estabrook, L. Iess, H. Wahlquist, and myself; I am particularly indebted to these colleagues for their work on this joint experiment and their perceptive comments on all aspects of the precision Doppler tracking problem. I am also grateful to R. Woo for continuing clarifying discussions on radiowave scintillation and M. J. Connally, R. G. Herrera, and P. Priest for essential contributions to the success of the MO, GLL, and MGS experiment planning and data taking. The research described here was carried out at the Jet Propulsion Laboratory, California Institute of Technology, under a contract with NASA.

References

Anderson, J. D., Armstrong, J. W., Campbell, J. K., Estabrook, F. B., and Lau, E. L. Gravitation and Celestial Mechanics Investigations with Galileo *Space Sci. Revs.*, 60, 591-610, 1992.

Anderson, J. D., Sjogren, W. L., and Schubert, G., Galileo Gravity Results and the Internal Structure of Io, *Science ,272, 709-712, 1996.*

Armstrong, J. W. Bispectral Analysis of Meter Wavelength Interplanetary Scintillation, *Astron. Astrophys. 61, 313-320,* 1977.

Armstrong, J. W., Woo, R., and Estabrook, F. B. Interplanetary Phase Scintillation and the Search for Very Low-Frequency Gravitational Radiation *Ap. J.*, 230, 570-574, 1979 (erratum *Ap. J. 240,719, 1980).*

Armstrong, J. W. and Sramek, R. A. Observations of Tropospheric Phase Scintillation at 5 GHz on Vertical Paths *Radio Science, 17, 1579-1586,* 1982.

Armstrong, J. W. Spacecraft Gravitational Wave Experiments in *Gravitational Wave Data Analysis,* edited by B. Schutz, pp. 153-172, Kluwer, Dordrecht, 1989.

Asmar, S. W. and Renzetti, N., The Deep Space Network as an Instrument for Radio Science Research, *JPL Publication 80-93, Rev. 1,* Pasadena CA, 1993.

Barnes, J. A. *et al.,* Characterization of Frequency Stability, *National Bureau of Standards Technical Note 394,* Boulder CO, 1970.

Bertotti, B., Comoretto, G., and Iess, L. Doppler Tracking of Spacecraft with Multifrequency Links, *Astron. Astrophys.*, *269, 608-616, 1993.*

Comoretto, G., Bertotti, B., Iess, L., and Ambrosini, R., Doppler Experiments with the Cassini Radio System, *Nuovo Cimento C, 15*, 1193-1198, 1992.

D'Addario, L. R., Time Synchronization in Orbiting VLBI, *IEEE Trans. Instrumentation and Measurement, 40,584-590, 1991.*

Estabrook, F. B. Gravitational Wave Detection with the Solar Probe. II. The Doppler Tracking Method, in *A Close-Up of the Sun* , edited by M. Neugebauer and R. W. Davies, pp. 441-449, JPL Publication 78-70, 1978.

Estabrook, F. B. and Wahlquist, H. D. Response of Doppler Spacecraft Tracking to Gravitational Radiation *Gen. Rel. Grav., 6,439-447, 1975.*

French, R. G., Elliot, J. L., French, L. M., Kangas, J. A., Meech, K. J., et al., Uranian Ring Orbits From Earth-Based and Voyager Occultation Observations, *Icarus, 73, 349-378, 1988.*

Helstrom, C. W., Statistical Theory of Signal Detection, Pergamon Press, Oxford, 1969.

Jenkins, G. M. and Watts, D. G., Spectral Analysis and Its Applications, Holden-Day, Sanfrancisco, 1969.

Keihm, S. J., Water Vapor Radiometer Measurements of the Tropospheric Delay Fluctuations at Goldstone over a Full Year, TDA *Progress Report, 42-122,* 1-11, 1995.

Kliore, A. J., Hinson, D. P., Flasar, F. M., Nagy, A. F., and Cravens, T. E., The Ionosphere of Europa From Galileo Radio Occultations, *Science, 277, 355-358, 1997.*

Kursinski , E. R. et *al.,* Initial Results of Radio Occultation Observations of Earth's Atmosphere Using the Global Positioning System, *Science,* 271, 1107-1110, 1996.

MacDonald, G. J. Spectral Analysis of Time-Series Generated by Nonlinear Processes, *Rev. Geophysics, 27,449-469, 1989.*

Marouf, E. A., Tyler, G. L., and Rosen, P., Profiling Saturn's Rings by Radio Occultation, *Icarus,* 68, 120-166, 1986.

Otoshi, T. Y., France, M. M., and Lutes, G. F., The Fractional Frequency Stability of a 34-m Diameter Beam Waveguide Antenna, *Proc. IEEE, 82,788-795, 1994.*

Peng, T. K., Armstrong, J. W., Breidenthal, J. C., Donivan, F. F., and Ham, N. C., Deep Space Network Enhancement for the Galileo Mission to Jupiter, *Acts Astronautic, 17, 321-330, 1988.*

Rappaport, N., Bertotti, B., Giampieri, G., and Anderson, J. D., Doppler Measurements of the Quadruple Moments of Titan, Icarus, 126,313-323, 1997.

Reasenberg, R. D. *et al.,* Viking Relativity Experiment: Verification of Signal Retardation by Solar Gravity *Ap. J.,* 234, L2 19-221, 1979.

Riley, A. L. et *al.*, Cassini Ka-Band Precision Doppler and Enhanced Telecommunications System Study, *Joint NASA/JPL/ASI study on Ku-band*, Jet Propulsion Laboratory, Pasadena CA, 1990.

Rogers, A. E. E., Moffet, A. T., Backer, D. C., and Moran, J. M., Coherence Limits in VLBI Observations at 3-millimeter Wavelength, *Radio Sci., 19, 1552-1560, 1984.*

Schubert, G., Limonadi, D., Anderson, J. D., Campbell, J. K., and Giampieri, G., Gravitational Coefficients and Internal structure of the Icy Galilean Satellites: An Assessment of the Galileo Orbiter Mission, Icarus, 111,433-440, 1994.

Sramek, R. A., Atmospheric Phase Stability at the VLA, *VLA Test Memorandum No. 175,* National Radio Astronomy Observatory, Charlottesville VA, 1989.

Tinto, M. and Armstrong, J. W., Spacecraft Doppler Tracking as a Narrow-Band Detector of Gravitational Radiation, to be submitted to *Phys. Rev., 1997.*

Thorne, K. S., Gravitational Radiation, in 300 *Years of Gravitation ,* edited by S. W. Hawking and W. Israel, pp. 330-458, Cambridge University Press, Cambridge, 1987.

Tyler, G. L. et *al.*, Radio Science Investigations with Mars Observer, *JGR, 97, 7759-7779, 1992.*

Vessot, R. F. C. and Levine, M. W., A Time-Correlated Four-Link Doppler Tracking System, in *A Close-Up of the Sun* , edited by M. Neugebauer and R. W. Davies, pp. 457-497, JPL Publication 78-70, 1978.

Vessot, R. F. C. *et al.,* Tests of Relativistic Gravitation with a Space-Borne Hydrogen Maser, *Phys. Rev. Lett., 45, 2081-2084, 1980.*

Vessot, R. F. C., Space Experiments with High Stability Clocks, in *Proceeding of the Workshop on the Scientific Applications of Clocks in Space,* edited by Lute Maleki, pp. 67-92, JPL Publication 97-15, 1977.

Wahlquist, H. D., Anderson, J. D., Estabrook, F. B., Thorne, K. S., Recent JPL Work on Gravity Wave Detection and Solar System Relativity Experiments, *Atti dei Covegni Lincei, 34, 335-350, 1977.*

Wahlquist, H. D. The Doppler Response to Gravitational Waves form a Binary Star Source, *Gen. Rel. Grav.,* 19, 1101-1113, 1987.

Wright, M. C. H., Atmospheric Phase Noise and Aperture-Synthesis Imaging at Millimeter Wavelengths, *Pub. Astron. Sot. Pacific, 108,520-534, 1996.*

Figure Captions

Figure 1. Four space-time diagrams illustrating transfer functions to the 2-way Doppler observable for clock noise, tropospheric scintillation, antenna mechanical noise, and charged particle (ionospheric, x = O, and solar wind scintillation). Space is plotted vertically and time is plotted horizontally; radio waves transmitted to and received from the spacecraft are shown as dashed lines. Under each diagram is a schematic time series of the Doppler signature produced by the indicated perturbation. The spacecraft transponder ratio (ratio of the downlink frequency to the uplink frequency) is α.

Figure 2. Example autocorrelation function of X-band Mars Global Surveyor data (1997 DOY 108, elongation = 1220). Inset is power spectrum with frequency axis labeled in units of $1/T_2$, where T_2 = 2 L/c is the two-way light time The well-defined peak in the autocorrelation function at $\tau = T_2$ is observed in $\gtrsim 90\%$ of the X-band data and is interpreted as due to tropospheric scintillation.

Figure 3. As Figure 2, but for S-band Galileo data on 1993 DOY 091 (elongation = 1450, T_2 = 801 seconds) low-pass filtered at 0.01 Hz prior to estimation of the correlation function. This is illustrative of positive correlation at τ = T2, which is observed about 60% of the time in Galileo's S-band data set.

Figure 4. As Figure 2, but for S-band Galileo data on 1993 DOY 090 (elongation = 1460, T_2 = 787 seconds). This illustrates a situation where there is no clear correlation at $\tau = T_2$.

Figure 5. As Figure 2, but for S-band Galileo data on 1993 DOY 098 (elongation = 139^o, T_2 = 901 seconds). This is an example of a well-defined correlation peak at $\tau <$ T2, presumably caused by a well-localized scattering region in the solar wind.

Figure 6. Allan deviation (τ = 100 seconds) of the solar wind (upper panel) and tropospheric(lower panel) noise under the assumption that the two processes are white in the $\approx$ 0.001-0.05 Hz band of the data. The dotted interval shows the average AlIan deviation expected from the troposphere at low elevations angles (normalized from a year of WVR data at

Goldstone; Keihm [1995]) and at an integration time of 200 seconds (the shortest integration time in the WVR analysis). The dotted line in the upper panel shows the Allan deviation of two-way Doppler expected at elongation = 100° for X-band charged particles [Armstrong, Woo, and Estabrook 1979, 1980].

J. W. Armstrong, Jet Propulsion Laboratory, California Institute of Technology, Mail Stop 238-725,4800 Oak Grove Dr., Pasadena CA 91109 (e-mail: john.w.armstrong @jpl.nasa.gov)

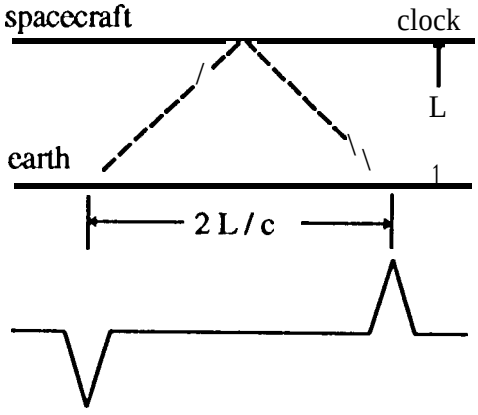
spacecraft
clock
L
earth
2 L / c

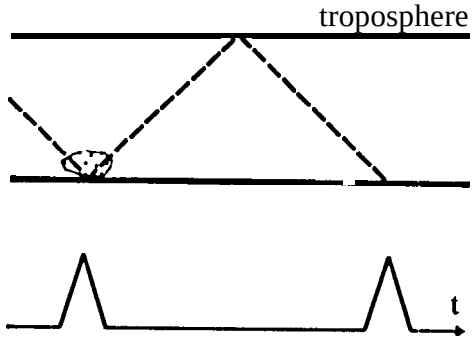
troposphere
t

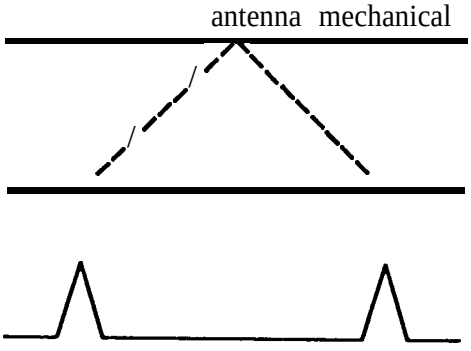
antenna mechanical

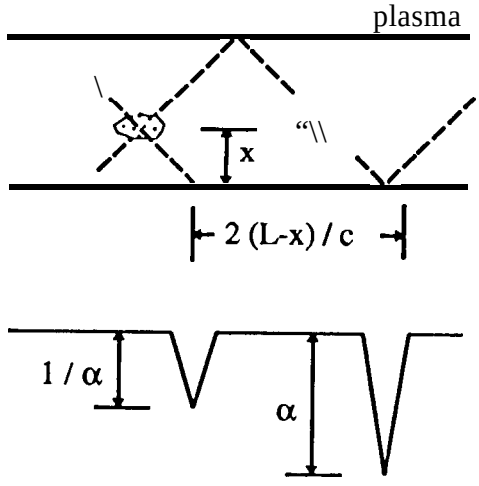
plasma
x
2 (L-x) / c
1 / α
α

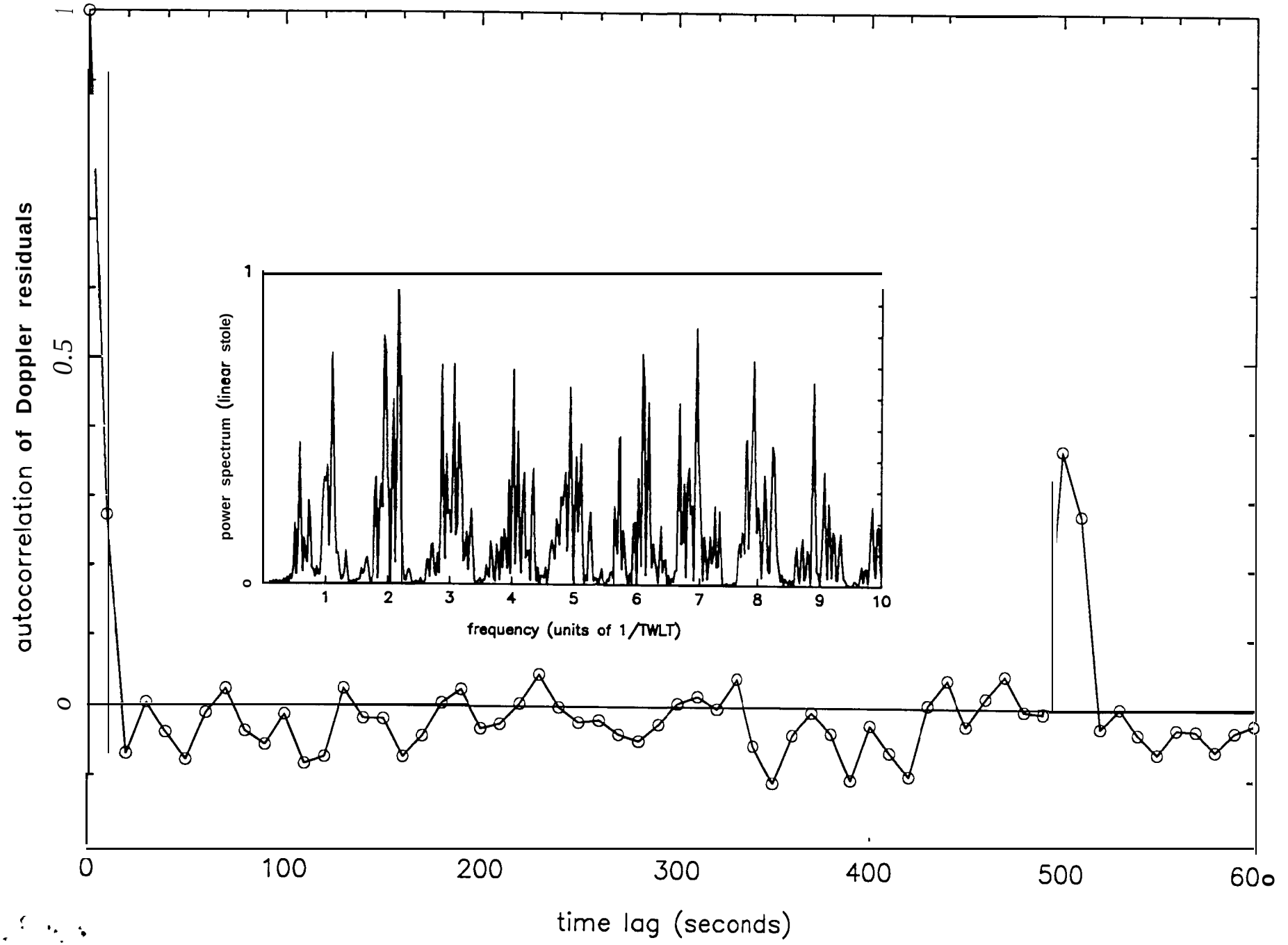
autocorrelation of Doppler residuals
1
0.5
0
0
100
200
300
400
500
600
time lag (seconds)
power spectrum (linear stole)
1
0
1
2
3
4
5
6
7
8
9
10
frequency (units of 1/TWLT)

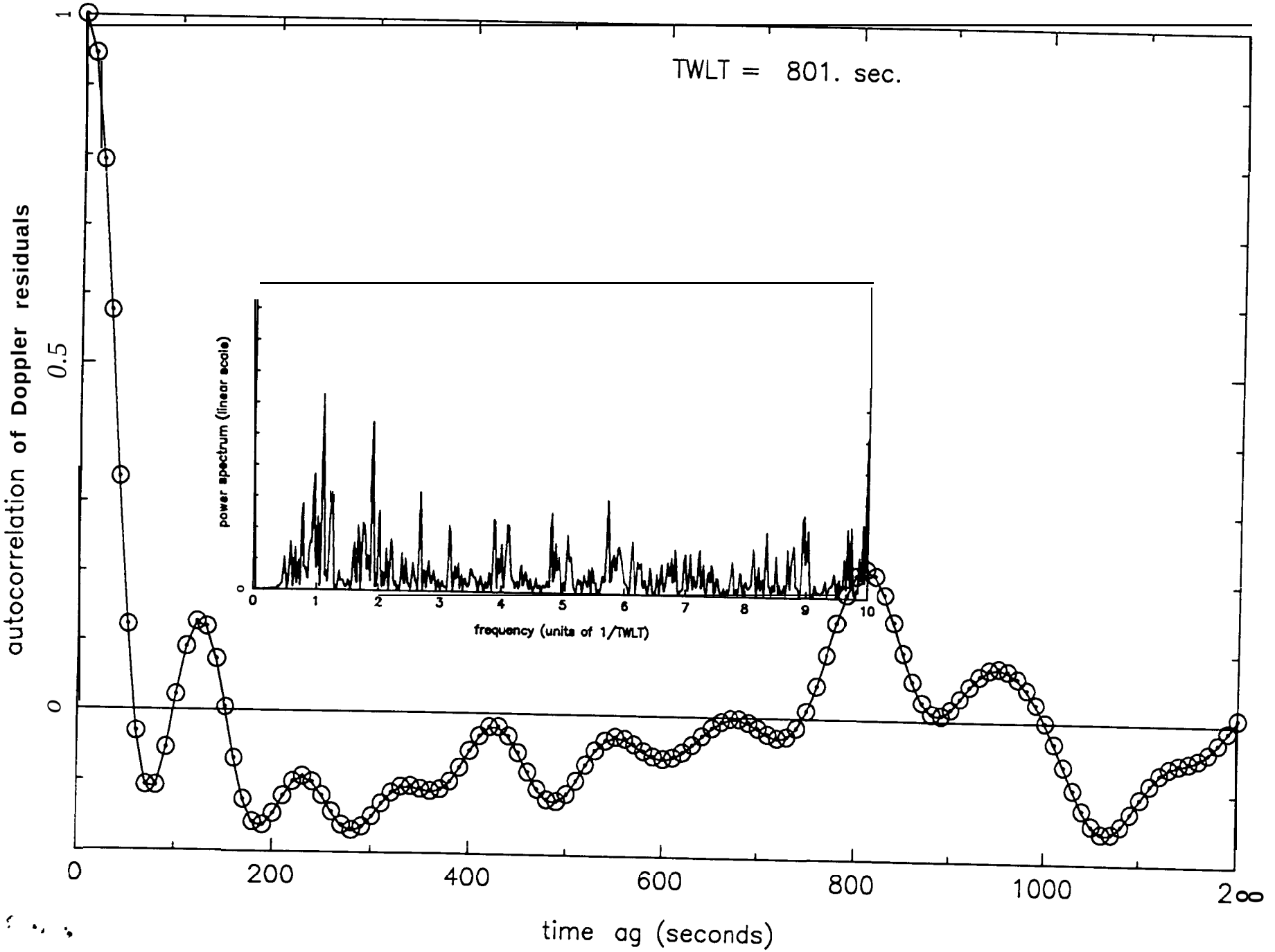
TWLT = 801. sec.
autocorrelation of Doppler residuals
1
0.5
0
0
200
400
600
800
1000
2∞
time ag (seconds)
power spectrum (linear scale)
0
0
1
2
3
4
5
6
7
8
9
10
frequency (units of 1/TWLT)

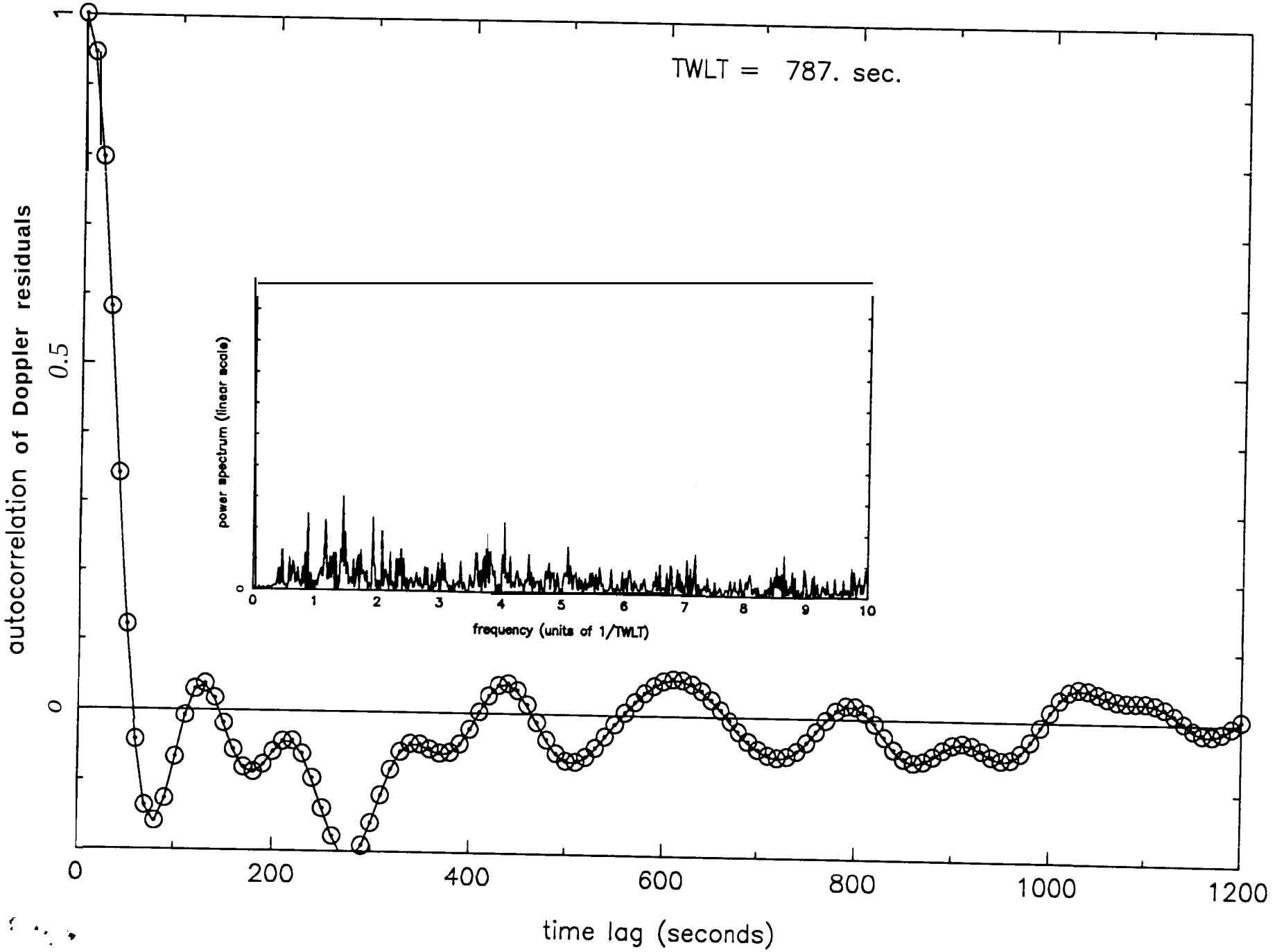
TWLT = 787. sec.
autocorrelation of Doppler residuals
1
0.5
0
0
200
400
600
800
1000
1200
time lag (seconds)
power spectrum (linear scale)
0
0
1
2
3
4
5
6
7
8
9
10
frequency (units of 1/TWLT)

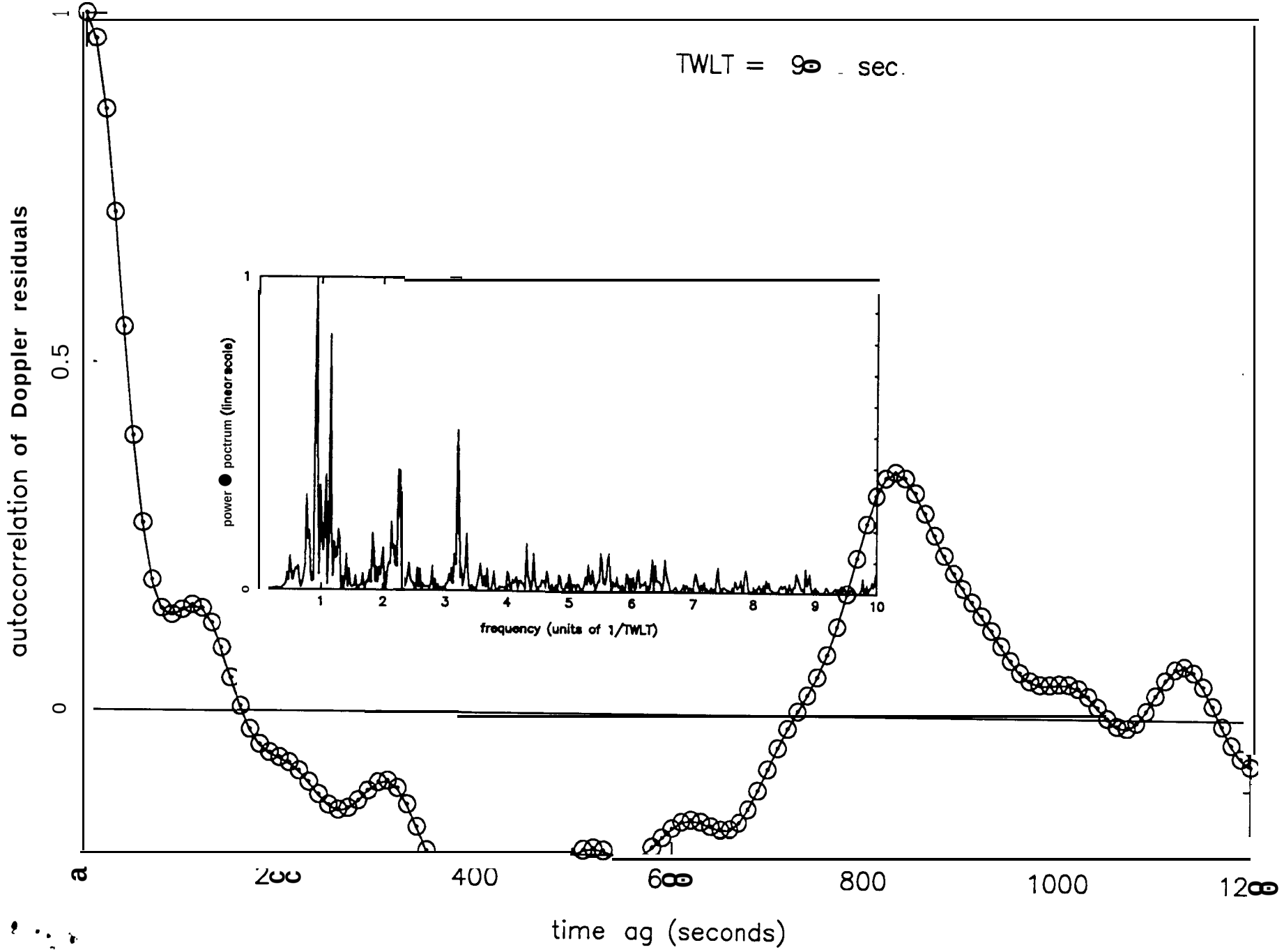
TWLT = 9∞ sec.
autocorrelation of Doppler residuals
1
0.5
0
power ● poctrum (linear scale)
1
0
1
2
3
4
5
6
7
8
9
10
frequency (units of 1/TWLT)
a
2∞
400
6∞
800
1000
12∞
time ag (seconds)

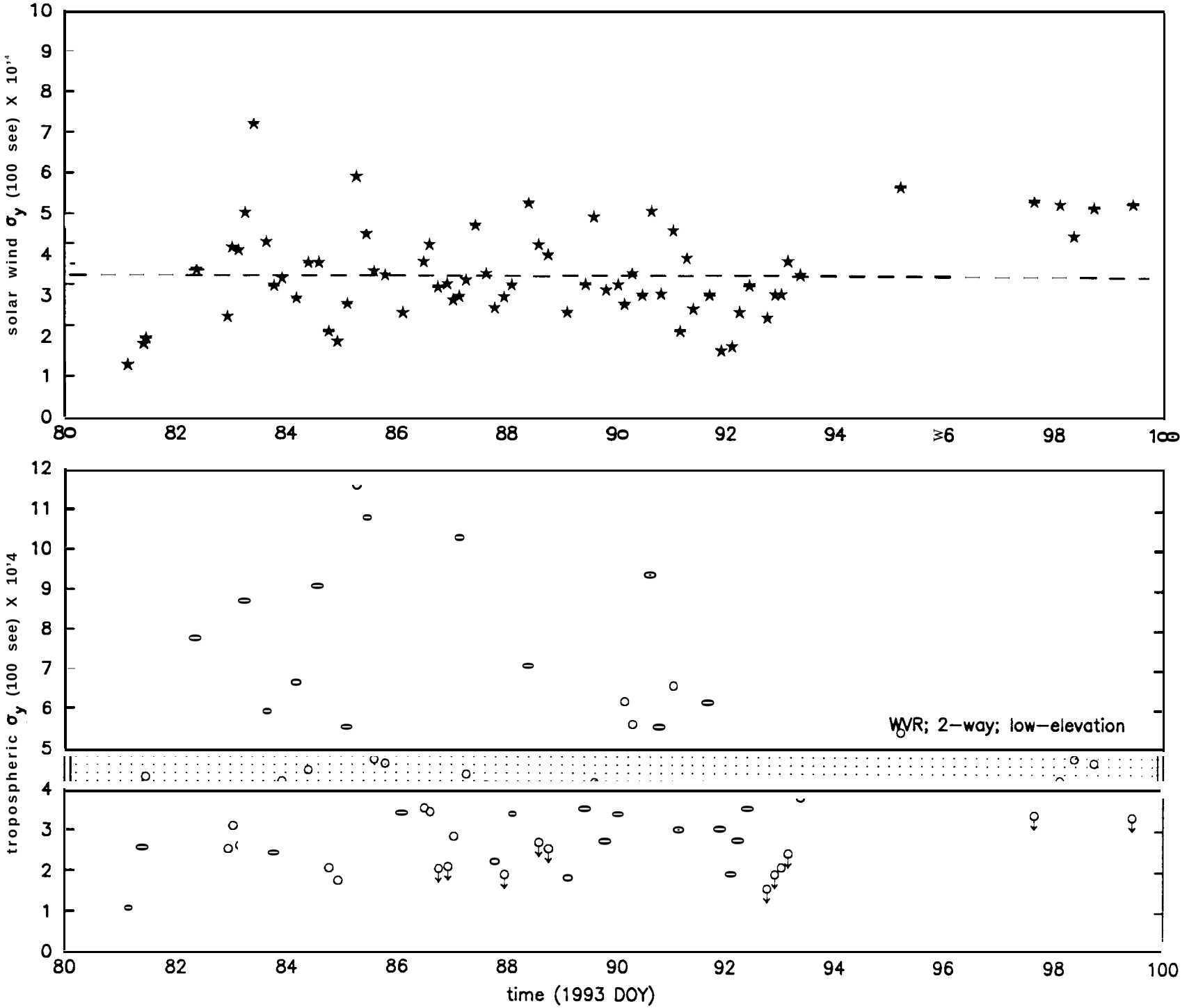
solar wind σ_y (100 sec) X 10^{-4}
troposphere σ_y (100 sec) X 10^{-4}
WVR; 2-way; low-elevation
time (1993 DOY)